Biophysical Chemistry 168–169 (2012) 10–18

Contents lists available at SciVerse ScienceDirect

Biophysical Chemistry

journal homepage: http://www.elsevier.com/locate/biophyschem

Thermodynamics of amyloid dissociation provide insights into aggregate stability regimes

Rebecca K. Brummitt [a,1], Jennifer M. Andrews [a,2], Jacob L. Jordan [b,3], Erik J. Fernandez [b], Christopher J. Roberts [a,*]

[a] Department of Chemical Engineering, University of Delaware, Newark, DE 19716, USA
[b] Department of Chemical Engineering, University of Virginia, Charlottesville, VA 22904, USA

HIGHLIGHTS

- General methodology to estimate thermodynamic stability of irreversible protein aggregates.
- Chymotrypsinogen amyloid is the lowest free energy state over only a limited regime.
- Kinetic stability of protein aggregates can dominate over thermodynamic stability.

GRAPHICAL ABSTRACT

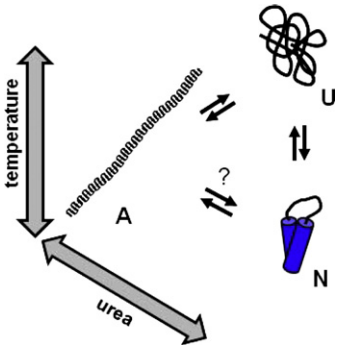

ARTICLE INFO

Article history:
Received 7 March 2012
Received in revised form 31 May 2012
Accepted 1 June 2012
Available online 7 June 2012

Keywords:
Amyloid dissociation
Amyloid stability
Thermodynamic integration
Calorimetry
Protein transfer free energy

ABSTRACT

Amyloid aggregates have been hypothesized as a global low free energy state for proteins at finite concentrations. Near its midpoint unfolding temperature, α-chymotrypsinogen A (aCgn) spontaneously forms amyloid polymers, indicating the free energy of aggregates (*A*) is significantly lower than that for unfolded (*U*) and native (*N*) monomers at those particular conditions. The relative thermodynamic stability of *A*, *U*, and *N* states was estimated semi-quantitatively as a function of temperature (*T*) and [urea] via a combination of calorimetry, urea-assisted unfolding and dissociation, aggregation kinetics, and changes in solvent-exposed surface area, combined with thermodynamic integration and a linear transfer free energy model. The results at first suggest that *N* is more thermodynamically stable than *A* at sufficiently low *T* and [urea], but this may be convoluted with kinetic effects. Interestingly, the kinetic stability of aggregates highlights that the practical measure of stability may be the free energy barrier(s) between *A* and *U*, as *U* serves as a key intermediate between *N* and *A* states.

1. Introduction

Non-native protein aggregation involves the assembly of initially monomeric protein into aggregates in which the constituent proteins have lost a significant portion of their native secondary structure. In addition, these structural changes at least putatively facilitate the formation of strong inter-protein contacts and non-native structures that make the aggregates effectively irreversible under the conditions that

* Corresponding author at: Department of Chemical and Biomolecular Engineering, University of Delaware, 223 Colburn Laboratory, 150 Academy St., Newark, DE 19716, USA. Tel.: +1 302 831 0838; fax: +1 302 831 1048.
E-mail address: cjr@udel.edu (C.J. Roberts).
[1] Current Address: U. S. Food and Drug Administration, Rockville, MD 20855, USA.
[2] Current Address: Biopharmaceutical Research and Development, GlaxoSmithKline, King of Prussia, PA 19406, USA.
[3] Current Address: Booz Allen Hamilton, Arlington VA 22203, USA.

0301-4622/$ – see front matter © 2012 Elsevier B.V. All rights reserved.
doi:10.1016/j.bpc.2012.06.001

they form [1–3]. Amyloid is a particular structural form or state of non-native aggregates, in which inter-protein contacts involve extended beta-sheet structures that stabilize aggregates via hydrogen bonds between strands on different protein molecules. Additionally, favorable burial of hydrophobic surfaces, as well as backbone and sidechain packing, contribute to amyloid stabilization [1,4]. Amyloid is sometimes considered to be a more stable conformational/aggregation state than even that of isolated, folded monomers under many conditions; this is based on the observation that a wide variety of protein sequences can form amyloid, and historically that amyloid aggregates are highly resistive to dissociation [5–8]. In many cases, dissociation requires extremes of temperature, pressure, and/or concentrations of chemical denaturants that may be beyond those sufficient to unfold the monomeric protein in isolation [9–11].

More recently, marginally stable amyloid states or alternative dissociation strategies have been increasingly identified and used to study the stability of amyloid as a means to better understand which interactions or specific amino acid contacts are important for (de)stabilizing aggregates [6,12,13]. However, quantifying the thermodynamics of non-native aggregate formation remains problematic in many situations, as directly observing equilibrated monomer-aggregate transitions is practically difficult in experiment if one cannot identify conditions where forward and reverse polymerization can be monitored simultaneously [11].

Often, non-native aggregate nucleation and polymerization are not easily reversible on practical time scales unless the aggregates are subsequently heated, pressurized, and/or incubated in high concentrations of chemical denaturants. With some notable exceptions [12–15], the aggregates do not dissociate measurably upon dilution or with changes in solvent pH or ionic strength. Even when dissociation conditions are identified, the processes of aggregation and/or dissociation can be under kinetic control on practical time scales, and therefore elucidating the quantitative thermodynamics of aggregation/dissociation requires alternative approaches. As such, an indirect approach to predict conditions that thermodynamically stabilize the native (N) or folded monomer state compared to the aggregate (A) state could provide insights into the mechanism(s) and driving forces by which aggregates form, as well as provide means to better control or eliminate aggregates that are a long-standing concern for biotechnology products such as therapeutic proteins [16].

The model system in the present report is α-chymotrypsinogen A (aCgn). aCgn is a natively monomeric, globular α/β protein that was previously shown to spontaneously form soluble amyloid polymers at acidic solution conditions and temperatures in the vicinity of the monomer midpoint unfolding temperature (T_M ~ 60 °C) on time scales of minutes to days [17,18]. Aggregation under these conditions proceeds via partial unfolding to populate molten-globule monomers that can first reversibly self-associate to form low levels of non-specific trimers and tetramers; those oligomers then nucleate net-irreversible amyloid aggregates that grow rapidly via monomer addition (i.e., chain polymerization) [17,19–21]. The resulting aggregates are akin to protofilaments, rather than fibrils, as they do not coalesce or bundle with one another unless one considers conditions of higher ionic strength and/or pH where aggregate–aggregate attractions become prominent [17,22].

In the present study, partial specific enthalpies versus temperature were determined via calorimetry, and combined with unfolding thermodynamics and aggregate dissociation kinetics to assess the relative chemical potential of aggregate (μ_A^{ex}, per monomer basis), folded or native monomer (μ_N^{ex}), and unfolded monomer (μ_U^{ex}) as a function of temperature for aCgn in the absence of urea. A separate assessment of aggregate stability under isothermal conditions near room temperature (26 °C) was also performed, using a combination of aggregate dissociation kinetics as a function of urea concentration, and estimates of relative exposed surface areas of A, N, and U from hydrogen–deuterium exchange monitored by mass spectrometry (HDX-MS) [23,24]. Results from these measurements were used to place bounds on the possible range of relative transfer free energy values for A, N, and U as a function of urea concentration, and were compared to predictions from temperature extrapolation in the absence of urea.

Together, the results indicate that although aggregates appear to be the free energy minimum for protein concentrations on the order of 10 micromolar over a range of temperature (T), the folded (unfolded) monomer is inferred to be more thermodynamically stable if one considers significantly lower (higher) temperatures in the absence of urea. Comparison between the estimated thermodynamic and observed kinetic stability of aggregates also highlights the importance of incorporating the free energy barriers separating A, N, and U states when considering a practical definition of aggregate stability. The approach employed here is expected to be applicable to other aggregation-prone proteins so as to estimate stability regimes for aggregates versus monomers.

2. Materials and methods

2.1. Protein solution preparation

10 mM sodium citrate buffer stock solutions were prepared by dissolving citric acid monohydrate (Fisher Scientific, Pittsburgh, PA, molecular biology grade) in distilled, deionized water, and titrating to pH 3.5 with 1 M sodium hydroxide solution (Fisher Scientific). Solutions of aCgn were prepared gravimetrically from 5× crystallized lyophilized aCgn (Worthington Biochemical Corp., Milford, MA) dissolved in aliquots of stock citrate buffer to yield a final protein concentration of either 1.2 or 2 mg/mL, with solution pH confirmed after protein dissolution.

Aggregated protein samples for subsequent dissociation experiments were prepared by thermostatting initially monomeric aCgn solutions at 65 ± 0.2 °C for a predetermined time to yield approximately 95% (by mass) aggregated protein [19,22]. Aggregated samples were quenched in an ice-water bath immediately after preparation for at least 5 min, to arrest further aggregation [17,19,21]. All protein solutions (aggregated and monomeric) were refrigerated (2–8 °C) and used within one week of preparation, during which time no further aggregation was detectable via size-exclusion chromatography or laser light scattering (data not shown).

2.2. Urea stock solutions

8.5 M urea stock solutions in 10 mM citrate buffer were prepared gravimetrically by combining urea (MP Biomedicals, Solon, OH, Ultra Pure) with citric acid monohydrate and distilled, deionized water. Hydrochloric acid (Fisher Scientific, ACS grade) was used to adjust the urea stock solution to pH 3.5. A polynomial expression that relates urea density to molality and temperature [25] was used to calculate molarity. Solutions were stored at −20 °C to minimize chemical degradation, and used within two weeks of preparation.

2.3. Differential scanning calorimetry (DSC)

Aggregate samples were prepared at 1.2 mg/mL as described above. A series of at least four buffer/buffer scans was used to establish instrument thermal history and to obtain the instrument baseline on a VP-DSC (Microcal, Northampton, MA). The average of these buffer/buffer scans was subtracted from each protein scan and the absolute, partial specific heat capacity (c_p) was determined using standard procedures [26]. Solvent properties were treated as being identical to those of water. The partial specific heat capacity of preformed aggregates was determined from scanning at 60 °C/h over a temperature range of 20 to 55 °C. This temperature range was chosen to conservatively ensure that the aggregates would not undergo temperature-induced dissociation during the scans [19], and to purposefully include the temperature of the isothermal calorimetry experiments (see below). The partial

specific volume of the aggregates was approximated as equal to that for folded monomer [27] (0.73 mL g^{-1}) for purposes of converting the DSC signals to absolute heat capacity values.

2.4. Isothermal calorimetry

Isothermal calorimetry was conducted with a VP-DSC operated in isothermal mode. The average of at least four buffer/buffer time-courses was used to obtain the instrument baseline prior to each sample measurement, and this baseline was subtracted from subsequent time-courses that included 2 mg/mL protein in the sample cell. To initialize a given isothermal experiment, the temperature was ramped from 15 to 55 °C over approximately 30 min. The temperature was then held constant at 55 ± 0.2 °C for the remainder of the experiment while the differential heat flow to sample and reference cells was recorded as an average every 5 s. Each experiment was performed in triplicate. 55 °C was selected as the operating temperature based on previously measured aggregation kinetics [19,22] that indicated aggregation would be prohibitively slow at lower temperatures, while at higher temperatures the initially monomeric protein material would aggregate almost completely during the heating and equilibration phases of the calorimeter.

The differential heat flow rate ($\dot{Q}_{obs}$) to the sample cell (relative to buffer control) was recorded as a function of sample incubation time under isothermal conditions, and related to the kinetics of aggregation via Eq. (1) (see also, Appendix A).

$$\dot{Q}_{\mathrm{obs}} = \left(\Delta\hat{H}_{\mathrm{un}} f_{\mathrm{un}} - \Delta\hat{H}_{\mathrm{agg}}\right) c_0 V_{\mathrm{cell}} \frac{dm}{dt} \tag{1}$$

In Eq. (1), c_0 denotes the total protein concentration, V_{cell} is the volume of the sample cell, and dm/dt is given by a rate expression such as Eq. (2) for aggregation of aCgn under these solution conditions [19,21,28,29].

$$\frac{dm}{dt} \cong -k_{\mathrm{obs}} m \tag{2}$$

In Eq. (2), m is the concentration of monomer divided by c_0, k_{obs} is the net or observed rate coefficient of aggregation for a given c_0, T, and solvent condition. Values for k_{obs} were determined previously via kinetics monitored chromatographically [17,19,21], and also confirmed separately here (see below).

For a given T, f_{un} in Eq. (1) is the fraction of monomer in the sample that is unfolded, $\Delta\hat{H}_{un}$ is the specific enthalpy change for monomer unfolding, $\Delta\hat{H}_{agg}$ is the difference in specific enthalpy between aggregate and folded or native monomer ($= \hat{H}_{agg} - \hat{H}_N$; described in more detail below). $\hat{H}_{agg}$ is approximated as being independent of aggregate polymer length, as all monomers in a linear polymer chain have roughly the same near-neighbor protein contacts and amount of solvent exposure, with the exception of monomers at the polymer termini. Because on average only a fraction (f_{un}) of monomers are unfolded at a given time t, and all enthalpies are taken relative to N, the term in parentheses in Eq. (1) therefore gives the value of the net enthalpy difference for converting between one gram of unfolded monomers and one gram of aggregated protein; note that dm/dt is negative, and thus the net process is for converting from monomer to aggregate.

Rather than assuming a value of k_{obs} when analyzing the isothermal calorimetry data, $\dot{Q}_{obs}$ versus t was also used to estimate m versus t using Eq. (3),

$$m = \frac{\dot{Q}_{\mathrm{obs}} - \dot{Q}_{\mathrm{obs},\infty}}{\dot{Q}_{\mathrm{obs},0} - \dot{Q}_{\mathrm{obs},\infty}} m_0 \tag{3}$$

where $\dot{Q}_{\mathrm{obs},\infty}$ is the heat signal at long time ($t \to \infty$), $\dot{Q}_{\mathrm{obs},0}$ is the initial signal, and $m_0 = m(t=0)$. In Eq. (3), only m and $\dot{Q}_{\mathrm{obs}}$ are functions of t. The values of m estimated from Eq. (3) were also compared to those determined independently from samples held isothermally and quenched at selected time intervals for analysis by size-exclusion chromatography (SEC), as described below.

2.5. Size-exclusion chromatography (SEC)

A Waters Alliance 2695 separations module with a Waters 2996 photodiode array detector and a Waters Protein-Pak 125 (7.8 × 300 mm) size-exclusion column was used to quantify monomer concentrations in solution. The column was held at room temperature (20–22 °C), with an isocratic mobile phase composed of 0.5% (v/v) phosphoric acid (Fisher Scientific, Pittsburgh, PA, Certified ACS grade) in distilled deionized water adjusted to pH 2.5 with 5 M sodium hydroxide (Fisher Scientific, ACS grade). The mobile phase flow rate was 1 mL/min. These conditions were previously determined to provide good separation between monomer and aggregate peaks without altering the aggregate size distribution or stability of the aggregates [17,19,21]. Monomer concentrations were calculated from integrated peak area at 280 nm using the Empower™ software (Waters, Milford MA), with calibration against external standards.

2.6. Dissociation with urea

To initiate aggregate dissociation with urea, aggregate samples at 1.2 mg/mL were diluted gravimetrically to 0.17 mg/mL protein and urea concentrations of 2 to 6 M using the urea stock solution and citrate buffer; higher and lower final protein concentrations were also tested and gave indistinguishable results (not shown). Aliquots (1.5 mL) were placed in individual HPLC vials (deactivated borosilicate glass, part # 186000273DV, Waters) and hermetically sealed with HPLC screw caps (part # 186000274, Waters). Samples were immediately placed in a temperature-controlled autosampler chamber (Waters, Alliance 2695) set to 26 °C for injection onto a size-exclusion column (described above) after a specified hold time. The concentration of aCgn monomer was monitored via SEC at selected time points over a 24-hour period.

2.7. Circular dichroism (CD) spectroscopy

Measurements were performed on a Jasco Inc. (Easton, MD) J-810 spectropolarimeter equipped with a Jasco PTC-424S Peltier temperature control unit. Spectra of 0.2 mg/mL aCgn were obtained from 260 to 190 nm using a scanning rate of 50 nm/min. Three spectra were obtained and averaged for each sample, and baseline subtracted using the corresponding spectrum of the solution without protein. Mean residue ellipticity (MRE) in deg-cm^2/dmol was calculated using Eq. (4),

$$MRE = \frac{0.1\theta_\lambda MW}{cdn_r} \tag{4}$$

where θ_λ is the ellipticity (mdeg) at wavelength λ, MW is the molecular weight of the monomer (g/mol), c is the solution concentration (mg/mL), d is the cuvette path length (cm), and n_r is the number of amino acid residues per monomer.

2.8. Intrinsic fluorescence

Equilibrium intrinsic fluorescence spectra were obtained with a Jasco J-810 spectropolarimeter with a FMO-427S fluorescence detector. The excitation wavelength was 280 nm, and emission was monitored from

300 to 450 nm. The spectral center of mass (*COM*) was calculated for each average spectrum, after baseline subtraction, using Eq. (5),

$$COM = \frac{\sum_{\lambda} I_{\lambda} \cdot {}^{1}\!/\!_{\lambda}}{\sum_{\lambda} I_{\lambda}} \tag{5}$$

where λ is the wavelength (nm) and I_λ is the emission intensity at λ.

2.9. Hydrogen–deuterium exchange with mass spectrometry (HDX-MS)

The number of solvent accessible residues was estimated as the number of HD-exchangeable amide backbone protons in the *A* and *N* states (on a per monomer basis) as determined from intact protein mass spectrometry for fully aggregated (>97%) or folded monomeric samples, respectively. Exchange was monitored over approximately two days to allow exchange of unfolding through slowly dynamic residues. The results were compared to the analogous result for the *U* state, obtained from HDX experiments performed in 6 M urea (for reference, the midpoint unfolding concentration of urea is 4 M at these conditions [19]. Details regarding the labeling and quenching protocols, as well as the mass spectrometry measurements were the same as those described previously [18].

2.10. Determination of enthalpies and chemical potentials in the absence of urea

The partial specific enthalpies for native, unfolded, and aggregated states ($i = N$, *U*, and *A*, respectively) were calculated by integrating the respective heat capacities with respect to temperature, using Eq. (6).

$$\hat{H}_i(T) = \hat{H}_{i,\mathrm{ref}} + \int_{T_0}^{T} \hat{c}_{p,i}\, dT \tag{6}$$

The reference state for $i = N$ was taken as zero enthalpy at $T = 20$ °C. The value of $\hat{c}_{p,i}$ was taken as independent of *T* for $i = U$ or *A*, while it was a linear function of *T* for $i = N$, and was determined directly from the low-*T* baseline in DSC. The value of $\hat{H}_{U,\mathrm{ref}}$ was set to assure that the experimental difference in enthalpy between *N* and *U* was recovered at the midpoint unfolding temperature ($T_0 = T_M$) from DSC [19]; similarly, that for $i = A$ was set to match the enthalpy change upon aggregation in the isothermal aggregation experiment described above ($T_0 = 55$ °C). All partial specific enthalpies or heat capacities were converted to partial molar enthalpies (on a per-monomer basis; indicated by overbars) by using the monomer molecular weight. The change in the chemical potential (μ) for each protein state *i* as a function of temperature was then calculated from the partial molar enthalpies using the Gibbs–Helmholtz equation [30]. The value of $\mu_{U,\ \mathrm{ref}}$ was set to zero at 26 °C, for parity with the calculations described in the next subsection. The value of $\mu_{F,\ \mathrm{ref}}$ was then set so as to make $\mu_F = \mu_U$ at the experimental T_M value, in the absence of urea. The reference μ value for *A* was set as described in the Results and discussion section. The procedure above also places μ_A on a per-monomer basis for easier numerical comparison with μ_N and μ_U; this is valid provided that the aggregates are linear polymers in which the degree of polymerization is much greater than 2. This assumption holds in what follows below, as the aggregates had an average degree of polymerization of order 10^2 ($\langle n \rangle = 120 \pm 15$ and polydispersity index<0.2 from laser scattering; not shown). Aggregates were created under common conditions prior to subsequent characterization by DSC, spectroscopy, SEC-MALS, or HDX.

2.11. Calculation of relative chemical potential as a function of urea concentration at 26 °C

The urea-unfolding "m" value (m_{urea}) is roughly proportional to the difference in SSA for *N* versus *U*, and is also related to the difference in the transfer free energy (ΔG_{tr}) from water to a 1 M urea solution for *N* versus *U* [31]. If one defines f_i as the fraction of amino acids that are significantly solvent exposed, n_{aa} as the number of amino acids in the protein sequence, and δg_{tr} as ΔG_{tr} per amino acid (averaged over the protein sequence), one can express m_{urea} in a form analogous to that in Ref. [31] by assuming that the change in SSA is proportional to the change in solvent accessible, amide backbone hydrogen atoms. This gives

$$m_{\mathrm{urea}} = \delta g_{\mathrm{tr}} (f_U - f_N) n_{\mathrm{aa}} \tag{7}$$

The fraction of exposed amino acids was determined using hydrogen–deuterium exchange for aCgn as described above. The values for f_U, f_N, and f_A were determined to be 1, 0.45, and 0.78, respectively, consistent with results reported elsewhere for aCgn [18]. For aCgn, $n_{\mathrm{aa}} = 245$, and m_{urea} was determined previously [19] to be approximately -2.5 kcal mol^{-1} M^{-1} and essentially independent of temperature near ambient conditions. From Eq. (7) with these values, δg_{tr} is essentially -20 cal/mol. An analogous approach to obtain δg_{tr} by averaging over each amino acid residue using the method of Bolen and co-workers [31] gave semi-quantitatively similar results (not shown). The value of δg_{tr} was then used in Eq. (8) to calculate the change in chemical potential for state *i* as a function of urea concentration (c_{urea})

$$\mu_i(c_{\mathrm{urea}}) = \mu_i(0) + \delta g_{\mathrm{tr}} n_{\mathrm{aa}} f_i c_{\mathrm{urea}} \tag{8}$$

where $\mu_i(0)$ denotes the chemical potential of state *i* at zero concentration of urea, for this temperature (26 °C). This is essentially a linear transfer-free-energy (LTFE) model akin to those used previously to analyze unfolding thermodynamics [32]. As such, it does not explicitly account for possible changes in polymer configurational entropy (e.g., for the aggregates) as the solvent quality changes with addition of urea; however, as the analysis of the transfer free energy results are only semi-quantitative and qualitative in the present case, this limitation does not alter the main conclusions below. To make all monomer chemical potential values negative, the reference point was set as $\mu_U(0) = 0$. The value of $\mu_N(0)$was set to assure the chemical potential difference between *N* and *U* equaled zero at the corresponding experimental [19] midpoint value for c_{urea} of 4 M. The value for $\mu_A(0)$was estimated as described in the Results and discussion section.

3. Results and discussion

3.1. Aggregate specific heat capacity

Partial specific heat capacity was determined for preformed aCgn aggregates using DSC as described above. The monomer fraction was measured both before and after the DSC scans via SEC to be $m = 0.03$, confirming that negligible aggregate dissociation occurred, and contributions to the heat capacity measurements from residual monomer could be neglected. The results are shown in Fig. 1, with a linear extrapolation of the average aggregate heat capacity up to 90 °C. The heat capacity data for a purely monomer sample versus temperature are reproduced from Ref. [19] for comparison, and include the unfolding transition centered at approximately 60 °C. Aggregation was suppressed kinetically in that case, by working at sufficiently low protein concentration to avoid aggregation on the time scale of the DSC measurement.

The native monomer heat capacity is a linear function of temperature, while the heat capacity of the unfolded state (i.e., high-temperature baseline for monomer) and that for the aggregate are

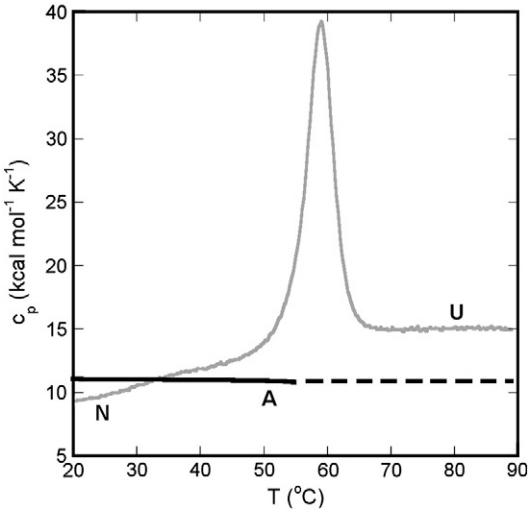

Fig. 1. Absolute heat capacity versus temperature for equilibrium unfolding (gray line) and aggregate (solid black line). The dashed lines represent the linear extrapolation of the aggregate heat capacity.

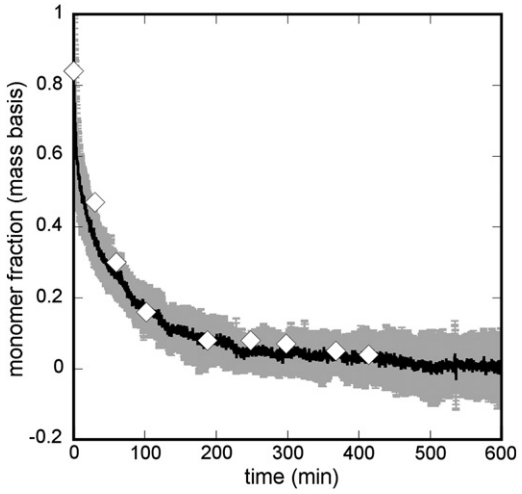

Fig. 2. Monomer fraction versus time for 2 mg/mL aCgn at 55 °C calculated from the heat signal from isothermal calorimetry and Eq. (3) (black line) and monitored by SEC (white diamonds). Error bars for the calorimetric data are represented by the gray region and account for the propagation of error from the terms in Eq. (3). The error bars for the SEC points are smaller than the symbols.

essentially independent of temperature over the range tested. The data in Fig. 1 show that the aggregate heat capacity is approximately 4 kcal mol^{-1} lower than that of unfolded monomers. The average value of the aggregate heat capacity over all temperatures is 11.0 ± 0.1 kcal mol^{-1} K^{-1} (on a per mole-of-monomer basis). Careful inspection of Fig. 1 shows that there is a small reduction in c_p for the aggregate as a function of temperature between 20 and 55 °C. Including this small temperature dependence to c_p for the aggregate does not appreciably change the results reported below.

3.2. Isothermal calorimetry to determine $\Delta\hat{H}_{agg}$

Isothermal calorimetry was used to monitor the heat evolved during aggregation of 1.2 and 2 mg/mL aCgn at 55 °C. Even at 55 °C, a small amount of aggregation (~10%) occurred during the 30 min heating plus equilibration period for the calorimeter, making the monomer fraction (m) equal 0.9 (based on SEC) at $t = 0$ for collection of $\dot{Q}_{obs}$. This loss was incorporated into the later analysis when comparing with isothermal kinetics from SEC, by using a value for m_0 in Eq. (3) based on SEC analysis of a sample that was heated in the DSC but removed and quenched on ice once the calorimeter began the kinetic portion of the run.

$\Delta\hat{H}_{un}$ and f_{un} as a function of temperature were determined previously from a 2-state fit of the equilibrium DSC data for monomer unfolding at low protein concentration [9]. $\Delta\hat{H}_{un}$ and f_{un} values for 55 °C were used in Eq. (1) when fitting isothermal $\dot{Q}_{obs}$ values versus time to obtain $\Delta\hat{H}_{agg}$ values. The confidence intervals of the fitted $\Delta\hat{H}_{agg}$ values for the 1.2 and 2.0 mg/mL conditions were calculated from the propagation of statistical errors in the terms in Eq. (1). The majority of the error is due to experimental uncertainty in the $\dot{Q}_{obs}$ data. At 55 °C, the enthalpy change upon converting one mole of monomers to aggregates was 37 ± 12 and 29 ± 5 kcal mol^{-1} for 1.2 and 2.0 mg/mL aCgn, respectively. Within statistical uncertainty, these values are the same for the two concentrations, and thus the averaged value of 33 kcal mol^{-1} was used in subsequent calculations.

Independent of the analysis of $\dot{Q}_{obs}$ via Eqs. (1) and (2), the fraction of monomer (m) versus time at 55 °C was estimated separately from $\dot{Q}_{obs}$ with Eq. (3) (see also Materials and methods). The results from Eq. (3) are shown in Fig. 2. The values of m vs time from separate samples that were incubated at 55 °C for different time periods, and then quenched on an ice-water bath and analyzed by SEC are also provided for comparison. The monomer fraction values calculated from the isothermal DSC data via Eq. (3) agree quantitatively with the SEC monomer loss profile, indicating that the assumptions in Eqs. (1) and (2) are reasonable for the conditions of the isothermal calorimetry measurements. k_{obs} was determined to be $(7.7 \pm 0.5) \times 10^{-3}$ min^{-1} by fitting the 2.0 mg/mL SEC monomer loss data to Eq. (2), in agreement with previous results [19].

3.3. Enthalpy and chemical potential versus temperature

Results for the partial molar enthalpy (per monomer basis) for each state (N, U, and A) calculated from Eq. (6) are shown in Fig. 3a. The reference state values are defined in the Materials and methods section. Fig. 3b shows enthalpy differences between the different protein states ($\bar{H}_U - \bar{H}_N, \bar{H}_A - \bar{H}_N$, *and* $\bar{H}_A - \bar{H}_U$). Fig. 4a shows the corresponding values for the chemical potential of N, U, and A states based on the enthalpy values in Fig. 3a, with the calculations described in Materials and methods. The absolute values for the chemical potential of A in Fig. 4a depends most sensitively on the choice of reference chemical potential, which was selected based on the considerations summarized immediately below, as well as the value of the enthalpy difference between monomer and aggregate at 55 °C (from Fig. 2). Those two quantities shift the family of curves in Figs. 3 and 4, while the temperature dependence (e.g. slopes and curvature changes with temperature) is ultimately derived from the heat capacity vs. temperature data (Fig. 1). There is small uncertainty in the heat capacity data (error bars of the order of the thickness of the lines in Fig. 1), while there is much larger uncertainty in the monomer-to-aggregate enthalpy change at 55 °C, and the reference point temperature noted below. As such, the curves in Fig. 4 should be considered semi-quantitative, as they could be shifted slightly if those reference point values are chosen differently within the uncertainty in those quantities.

In previous work, temperature-jump experiments indicated that aggregates formed below approximately 65 °C dissociated when subsequently jumped to significantly higher temperatures (~75 to 90 °C), while aggregates created at approximately 70 °C or higher temperature did not dissociate significantly when jumped to a higher temperature [9]. Similarly, in the present study, aggregates created at temperatures near T_M were slowly heated (~0.025 °C/min) and found to not dissociate (via SEC) until approximately 70 °C (data not shown). However, the kinetics of aggregate dissociation and re-aggregation were too slow to practically allow a true equilibrium point to be identified. As a result, the aggregate curve in Fig. 4a was drawn in a location such that

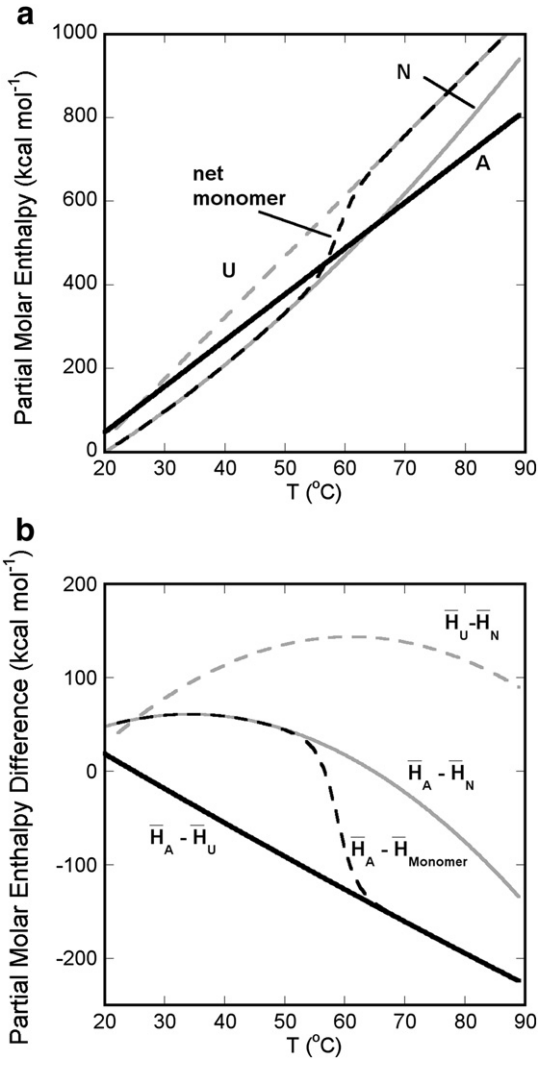

Fig. 3. (a) $\bar{H}_i - \bar{H}_N^{T=20C}$ versus temperature for native (solid gray line), unfolded (dashed gray line), monomer (dashed black line), and aggregate (solid black line). (b) $\Delta\bar{H}$ versus temperature for $\bar{H}_U - \bar{H}_N$ (dashed gray line), $\bar{H}_A - \bar{H}_N$ (solid gray line), $\bar{H}_A - \bar{H}_U$ (solid black line), and $\bar{H}_A - \bar{H}_M$ (dashed black line). All molar enthalpies are on a per-monomer basis.

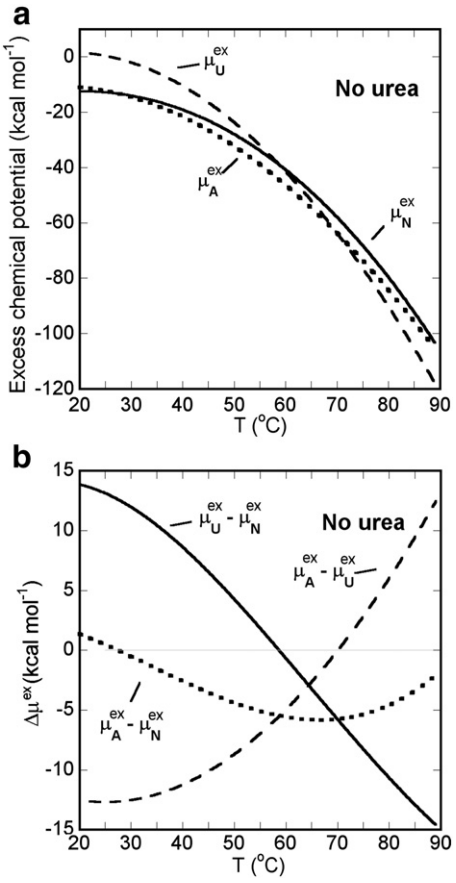

Fig. 4. (a) μ_i versus temperature with $\mu_{U\ (T=26C)} = 0$ for native (solid line), unfolded (dashed line), and aggregate (dotted line). (b) $\Delta\mu$ versus temperature for N➔U (solid line), U➔A (dashed line), and N➔A (dotted line).

it crossed the unfolded monomer curve at 70 °C, simply as an estimate to be consistent with the experimental observations listed above. Therefore, as noted above, the discussion and conclusions below are only semi-quantitative with regards to the calculated stability of *A* compared to *N* or *U*.

Fig. 4b shows the corresponding chemical potential differences among the three protein states ($\mu_U - \mu_N$, $\mu_A - \mu_U$, *and* $\mu_A - \mu_N$) based on the values in Fig. 4a. Inspection of Fig. 4 shows that the chemical potential of the aggregated state at these solvent conditions and protein concentration is predicted to be lower than that of the dominant monomer state (*N* or *U*) over a range of temperatures between approximately 30 and 70 °C. Based on the above discussion, the precise range of temperatures may shift slightly if one chooses to have the chemical potential of *A* and *U* cross at a temperature other than 70 °C.

The analysis leading to Fig. 4 shows that differences in c_p lead naturally to temperature-dependent differences in enthalpy and free energy between aggregate and monomer states, analogous to those between *N* and *U* states for monomers. Thus, it is perhaps not surprising that *A* would be stable only over a finite range of temperatures. Although beyond the scope of this study, the results in Figs. 3 and 4 suggest that if one were to cool sufficiently to induce cold unfolding of monomers, aggregates would still be disfavored compared to (now unfolded) monomers. This follows because c_p is highest for *U*, and the enthalpy of *U* is lowest at low temperatures; by the van't Hoff relation [30], equilibrium favors the lowest enthalpy (and entropy) state(s) as *T* is decreased.

3.4. aCgn unfolding and aggregate dissociation in urea

Urea-induced dissociation was also investigated at low temperature (26 °C), as a means to probe the relative experimental stability of *A* compared to *N* and *U* for aCgn. Time-dependent monomer recovery from aCgn aggregates incubated isothermally at selected urea concentrations was determined via SEC, as described above. Illustrative results are shown in Fig. 5a, and indicate that an increase in urea concentration resulted in a significant increase in the initial rate and overall extent of monomer recovery. Analogous experiments at lower and higher protein concentrations showed identical results within statistical uncertainty (not shown), indicating the dissociation process was under kinetic control. Thus, it was not viable to estimate a rate for reversal of dissociation, or an equilibrium extent of dissociation, under these conditions.

Measureable monomer recovery occurred for urea concentrations greater than approximately 2 M, and aggregates were clearly unstable above approximately 3 M urea. As these samples were only measured over 24 h, it is possible that aggregates would be unstable at lower urea concentrations if one were to wait for much longer time scales. Empirical evidence from this study (not shown) and previous work [17,19,20] indicated that aggregates show no discernable dissociation via SEC and/or light scattering on time scales of the order of weeks to

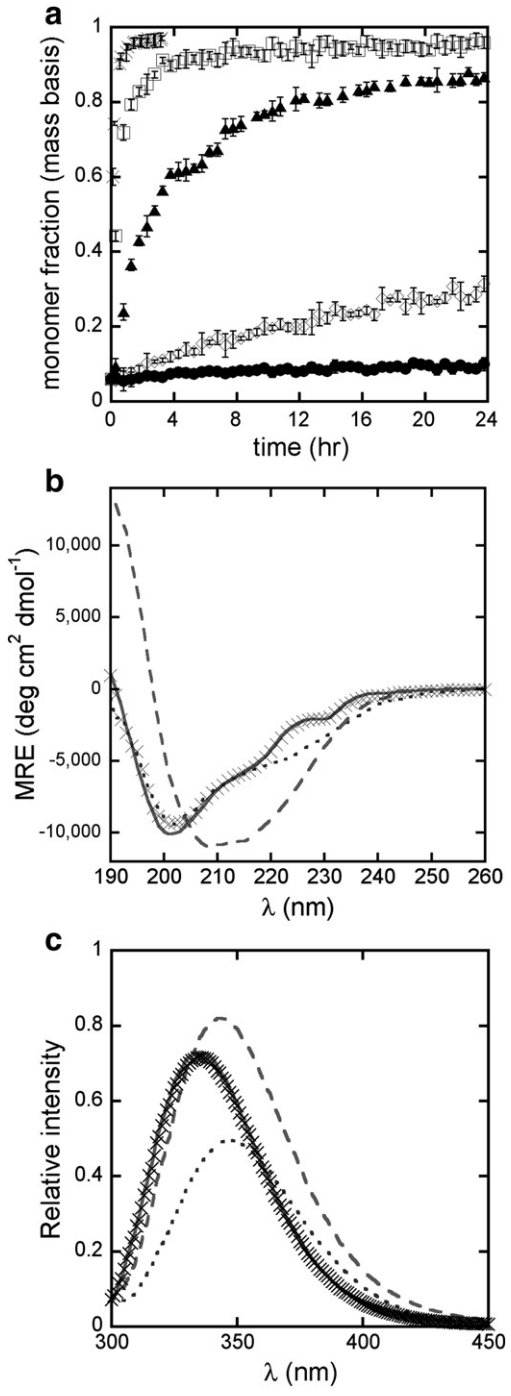

Fig. 5. (a) Monomer recovery over a 24-hour period for $c_0 = 1.2$ mg/mL aCgn dissociated in 2 M (closed squares), 3 M (open diamonds), 4 M (closed triangles), 5 M (open squares), and 6 M (x) urea at 26 °C. (b) Circular dichroism and (c) intrinsic fluorescence spectra for native monomer (solid line), unfolded monomer (dotted line), aggregate (dashed line), and protein that had been exposed to 4 M urea to promote dissociation of the aggregate and then dialyzed to remove the urea (crossed line).

months at room temperature or refrigerated in the absence of urea at this pH and ionic strength.

In order to assess whether dissociated monomers are able to refold to the parent monomer structure, CD and intrinsic fluorescence spectra were compared for *A*, *N*, and *U* states, as well as monomers recovered from dissociation of aggregates. Illustrative CD spectra are shown in Fig. 5b for native and thermally unfolded monomeric aCgn (low protein concentration) compared to aggregate that was created at pH 3.5 and 65 °C at a protein concentration of 2 mg/mL prior to dilution for purposes of the CD measurements. Also shown are spectra for aCgn that was first aggregated, then dissociated back to monomer in 4 M urea at 26 °C, and finally dialyzed to remove the urea before obtaining the CD spectrum. The spectra indicate a significant change in secondary structure from monomeric to aggregated protein. The aggregate secondary structure has some degree of elevated β-sheet content based on the red shift and a broad minimum near 212 nm, consistent with previous results [19]. The monomer secondary structure after dissociation and dialysis is essentially the same as the original native structure.

Analogous results from intrinsic fluorescence are shown in Fig. 5c for the same conditions as in Fig. 5b. The spectra show a red shift in spectral center of mass (COM) upon comparison of native monomer ($COM^{-1} \approx 343$ nm) with aggregate ($COM^{-1} \approx 351$ nm) or unfolded monomer ($COM^{-1} \approx 353$ nm). These shifts are consistent with those expected due to increased solvent exposure around tryptophan residues, although these data cannot distinguish which or how many tryptophan residues are exposed in aggregate versus unfolded states. The COM and the overall spectrum of the monomer after dissociation and dialysis to native-favoring conditions are the same as for those for native monomer prior to aggregation, indicating the monomers that are recovered from aCgn aggregates are able to refold.

3.5. Chemical potential versus urea concentration

The dependence of monomer and aggregate chemical potentials on urea concentration was estimated based on differences in number of exposed and exchangeable amide backbone hydrogen atoms (see also Materials and methods). This approach is an experimental alternative to estimating SSA from theoretical approaches, as the detailed three-dimensional structures of aggregates are not typically known. A low-resolution structure for aCgn aggregates was recently suggested [18], but the large majority of the structure is only approximate or putative, and was based on HDX measurements analogous to those performed here. As such, the HDX approach described above was considered a more robust and experimentally direct means to estimate relative differences in SSA.

Changes in chemical potential vs. urea concentration were therefore calculated from Eq. (8), with the results shown in Fig. 6a. As described in the Materials and methods section, the curves for the chemical potentials of *N* and *U* cross at 4 M urea, the experimental midpoint unfolding concentration at this temperature. The differences in the slopes of the curves are set by the differences in SSA estimated from HDX measurements, along with the experimental m_{urea} value for monomer unfolding. Thus the slope is greatest for *U*, smallest for *N*, and intermediate for *A*. Qualitatively, this ranking is also what is expected based on the relative degree of fluorophore exposure for *N*, *U*, and *A* indicated by the FL results in Fig. 5c. This is also consistent with the relative values of c_p for *N*, *U*, and *A* at low temperature, in that c_p for globular proteins scales roughly according to the amount of SSA [32].

The intercept for μ_A is not known exactly, but can be estimated or at least bounded via the results in Fig. 5a. Specifically, the observation that aggregates are unstable in urea concentrations of at least 4 M or higher indicates that the μ_A curve should not lie significantly lower (on the vertical axis) than where it is depicted in Fig. 6a, and the curve as drawn is taken as a reasonable lower bound. It also indicates that the chemical potential of *A* is higher than that for *N* at 26 °C, consistent with the predictions from calorimetry in Fig. 4.

Overall, the results in Figs. 4 and 6 are consistent with a model in which the degree of solvent exposure of protein backbone and hydrophobic side chains is significantly different between *N*, *U*, and *A* states for aCgn. This leads to significant differences in heat capacity and ΔG_{tr} for these three states, with both of these quantities increasing (at least qualitatively) with increasing SSA. The analysis associated with Fig. 6

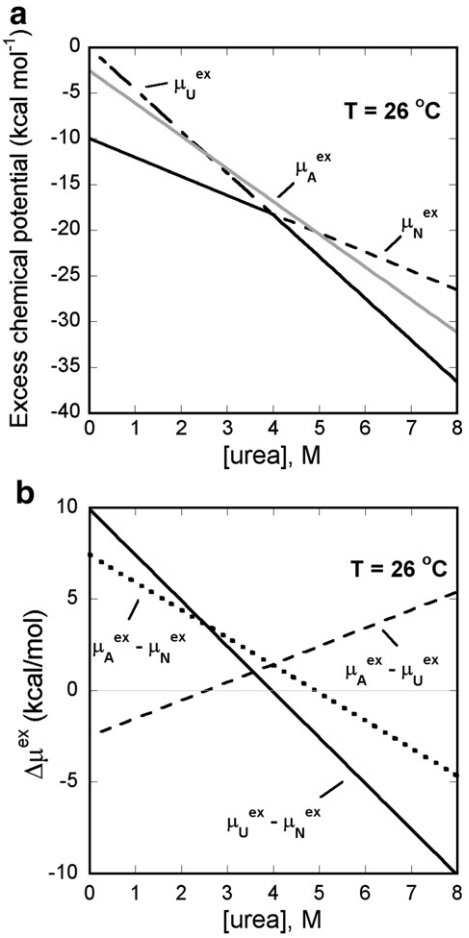

Fig. 6. (a) μ_i versus urea concentration with $\mu_{U\ (T=26C)} = 0$ for native (dashed line), unfolded (dotted-dashed line), monomer (solid black line), and aggregate (solid gray line). (b) $\Delta\mu$ versus urea concentration for N➔U (solid line), U➔A (dashed line), and N➔A (dotted line).

is based on a model in which ΔG_{tr} is linearly related to SSA, but qualitatively similar conclusions would be reached if ΔG_{tr} was slightly nonlinear, especially given the relatively limited experimental range of accessible c_{urea} values. From a qualitative perspective, if one is able to argue or show that aggregation results in significant burial of SSA compared to *U*, but that *N* retains the lowest SSA, then the qualitative picture in Fig. 6 is expected to hold as long as the minimal concentration of urea needed to destabilize aggregates lies at or below c_{mid} for monomer unfolding. Interestingly, if the μ_A curve were to shift vertically downwards in Fig. 6, that would suggest that for some protein systems the aggregates are more thermodynamically stable than monomers near c_{mid}, but less stable at higher and lower urea concentrations.

3.6. Comparing thermodynamic and kinetic effects on relative stability

In addition to the thermodynamic stability arguments presented above, one must also consider the empirical observation that aggregates of aCgn are apparently very kinetically stable (i.e., no measureable dissociation) on long time scales (of order 10–10^2 days) at refrigerated to room temperature conditions, in the absence of urea. Although the analysis above was only semi-quantitative, the results from calorimetry and estimated SSA differences qualitatively indicate that aggregates are ultimately expected to be unstable, relative to folded monomeric aCgn, at sufficiently low temperature.

This highlights that one must also factor in kinetic effects when considering how to define aggregate stability. For example, thermodynamic analysis assumes that there are no significant kinetic barriers to surmount in order to transfer from *A* to *N*, when concluding that *N* is more stable than *A* at low temperatures (i.e., our calculations assume true equilibrium is achieved). However, from a mechanistic perspective, a protein chain that is part of *A* must first dissociate before it can refold. As such, *U* or some sub-ensemble of conformers within the unfolded ensemble appear to be requisite intermediates on the pathway between *A* and *N*. If so, then the free energy barrier between *A* and *U* may be the more relevant quantity for defining practical measures of aggregate stability under strongly native-favoring conditions.

Furthermore, inspection of Fig. 4 shows that $\mu_A \ll \mu_U$ at room temperature and somewhat below. Thus, if *U* monomers are formed (even transiently) under these low temperature, native-favoring conditions, converting from *U* to *A* is very favorable thermodynamically. Therefore, it will be the relative free energy barriers for converting from *U* to either *A* or *N* that may dictate whether aggregates form on a given time scale. At temperatures near T_M, where both *N* and *U* are similarly populated, this may not be as much of a determining factor. Finally, the kinetics for converting to aggregates from any monomer state must be concentration dependent unless the transition from *N* to *U* is rate-limiting [33]. This further illustrates the need to consider the impact of kinetics, mechanisms, and free energy barriers if one is concerned with the process of preventing aggregation during prolonged protein storage. However, the thermodynamic analysis and approach illustrated here is promising if one is concerned with identifying the range of conditions where aggregates are thermodynamically favorable—e.g., so as to avoid those conditions when attempting to refold monomers or dissociate aggregates from inclusion bodies [34].

4. Conclusions

Results from a thermodynamic analysis of the relative calculated stabilities of folded monomer, unfolded monomer, and amyloid aggregate states for aCgn show that aggregates are expected to be thermodynamically favorable at intermediate temperatures, but not at high or low temperature in the absence of urea. The addition of urea at room temperature also shifts the experimentally observed stabilities of the various protein states; however, the aggregate is predicted to never be the most thermodynamically (rather than kinetically) stable state at the low temperature conditions examined. The general arguments given here regarding the effects of temperature and/or urea are not specific to aCgn or amyloid, and suggest that the precise range of thermodynamic stability for aggregates of a given protein will be limited, and may or may not include biologically or technologically relevant conditions. The results also highlight the importance of considering kinetic barriers when considering practical definitions of protein stability at low temperatures, where the dynamics of key steps in the association/dissociation process may control the observed behavior.

Acknowledgments

Financial support for RKB is gratefully acknowledged from the National Science Foundation (DGE 0221651). The funding sponsor did not partake in design, interpretation, or implementation of the experiments and analysis performed here, and was not involved in writing or submitting this report.

Appendix A

Eqs. (A1)–(A3) apply to isothermal calorimetry monitoring the kinetics of aggregation for a simple three-state model where native monomer (*N*), unfolded monomer (*U*), and aggregate (*A*) are the possible states. The measured rate of heat input or removal, as a function

of time (t) is expressed based on a differential form of the first law of thermodynamics

$$\dot{Q}_{obs} = \frac{dH}{dt} = \sum_i \frac{d\left(M_i \hat{H}_i\right)}{dt} \tag{A1}$$

Realizing that the partial specific enthalpy values for each of the i states does not depend on time for an isothermal, isobaric experiment at fixed solvent composition and low protein concentrations, Eq. (A1) becomes

$$\dot{Q}_{obs} = \frac{dM_N}{dt}\widehat{H}_N + \frac{dM_U}{dt}\widehat{H}_U + \frac{dM_A}{dt}\widehat{H}_A \tag{A2}$$

Using the mass balance $M_{tot} = C_0 V_{cell} = M_N + M_U + M_A$, and monomer mass defined as $M_{mon} = M_N + M_U$, Eq. (A2) can be simplified to

$$\dot{Q}_{obs} = \frac{dM_U}{dt}\left(\widehat{H}_U - \widehat{H}_N\right) + \frac{dM_{mon}}{dt}\left(\widehat{H}_N - \widehat{H}_A\right) \tag{A3}$$

Finally, substituting for M_{mon} and defining $\Delta H_{un} \equiv \widehat{H}_U - \widehat{H}_N$ and $\Delta H_{agg} \equiv \widehat{H}_A - \widehat{H}_N$, Eq. (A3) can be rewritten as Eq. (1) in the main text.

References

[1] C.M. Dobson, Principles of protein folding, misfolding and aggregation, Seminars in Cell & Developmental Biology 15 (2004) 3–16.
[2] A.L. Fink, Protein aggregation: folding aggregates, inclusion bodies and amyloid, Folding and Design 3 (1998) R9–R23.
[3] W.F. Weiss, T.M. Young, C.J. Roberts, Principles, approaches, and challenges for predicting protein aggregation rates and shelf life, Journal of Pharmaceutical Sciences 98 (2009) 1246–1277.
[4] D. Eisenberg, R. Nelson, M.R. Sawaya, M. Balbirnie, S. Sambashivan, M.I. Ivanova, A.Ø. Madsen, C. Riekel, The structural biology of protein aggregation diseases: fundamental questions and some answers, Accounts of Chemical Research 39 (2006) 568–575.
[5] A.J. Baldwin, T.P.J. Knowles, G.G. Tartaglia, A.W. Fitzpatrick, G.L. Devlin, S.L. Shammas, C.A. Waudby, M.F. Mossuto, S. Meehan, S.L. Gras, J. Christodoulou, S.J. Anthony-Cahill, P.D. Barker, M. Vendruscolo, C.M. Dobson, Metastability of native proteins and the phenomenon of amyloid formation, Journal of the American Chemical Society 133 (2011) 14160–14163.
[6] F. Meersman, C.M. Dobson, Probing the pressure-temperature stability of amyloid fibrils provides new insights into their molecular properties, Biochimica et Biophysica Acta, Proteins and Proteomics 1764 (2006) 452–460.
[7] E. Gazit, The "correctly folded" state of proteins: is it a metastable state? Angewandte Chemie International Edition 41 (2002) 257–259.
[8] J.D. Schmit, K. Ghosh, K. Dill, What drives amyloid molecules to assemble into oligomers and fibrils? Biophysical Journal 100 (2011) 450–458.
[9] B. Morel, L. Varela, F. Conejero-Lara, The thermodynamic stability of amyloid fibrils studied by differential scanning calorimetry, The Journal of Physical Chemistry. B 114 (2010) 4010–4019.
[10] D. Foguel, M.C. Suarez, A.D. Ferrao-Gonzales, T.C.R. Porto, L. Palmieri, C.M. Einsiedler, L.R. Andrade, H.A. Lashuel, P.T. Lansbury, J.W. Kelly, J.L. Silva, Dissociation of amyloid fibrils of α-synuclein and transthyretin by pressure reveals their reversible nature and the formation of water-excluded cavities, Proceedings of the National Academy of Sciences of the United States of America 100 (2003) 9831–9836.
[11] J. Kardos, A. Micsonai, H. Pal-Gabor, E. Petrik, L. Graf, J. Kovacs, Y. Lee, H. Naiki, Y. Goto, Reversible heat-induced dissociation of β2-microglobulin amyloid fibrils, Biochemistry 50 (2011) 3211–3220.
[12] R.P. McGlinchey, J.M. Gruschus, A. Nagy, J.C. Lee, Probing fibril dissolution of the repeat domain of a functional amyloid, Pmel17, on the microscopic and residue level, Biochemistry 50 (2011) 10567–10569.
[13] Z. Ye, D. Bayron Poueymiroy, J.J. Aguilera, S. Srinivasan, Y. Wang, L.C. Serpell, W. Colón, Inflammation protein SAA2.2 spontaneously forms marginally stable amyloid fibrils at physiological temperature, Biochemistry 50 (2011) 9184–9191.
[14] A. Top, C.J. Roberts, K.L. Kiick, Conformational and aggregation properties of a PEGylated alanine-rich polypeptide, Biomacromolecules 12 (2011) 2184–2192.
[15] A. Top, K.L. Kiick, C.J. Roberts, Modulation of self-association and subsequent fibril formation in an alanine-rich helical polypeptide, Biomacromolecules 9 (2008) 1595–1603.
[16] W. Wang, C. J. Roberts, and Editors, Aggregation of Therapeutic Proteins. John Wiley & Sons, Inc. 2010.
[17] W.F. Weiss, T.K. Hodgdon, E.W. Kaler, A.M. Lenhoff, C.J. Roberts, Nonnative protein polymers: structure, morphology, and relation to nucleation and growth, Biophysical Journal 93 (2007) 4392–4403.
[18] A. Zhang, J.L. Jordan, M.I. Ivanova, W.F. Weiss, C.J. Roberts, E.J. Fernandez, Molecular level insights into thermally induced α-chymotrypsinogen A amyloid aggregation mechanism and semiflexible protofibril morphology, Biochemistry 49 (2010) 10553–10564.
[19] J.M. Andrews, C.J. Roberts, Non-native aggregation of α-chymotrypsinogen occurs through nucleation and growth with competing nucleus sizes and negative activation energies, Biochemistry 46 (2007) 7558–7571.
[20] J.M. Andrews, W.F. Weiss, C.J. Roberts, Nucleation, growth, and activation energies for seeded and unseeded aggregation of α-chymotrypsinogen A, Biochemistry 47 (2008) 2397–2403.
[21] Y. Li, W.F. Weiss, C.J. Roberts, Characterization of high-molecular-weight non-native aggregates and aggregation kinetics by size exclusion chromatography with inline multi-angle laser light scattering, Journal of Pharmaceutical Sciences 98 (2009) 3997–4016.
[22] Y. Li, B.A. Ogunnaike, C.J. Roberts, Multi-variate approach to global protein aggregation behavior and kinetics: effects of pH, NaCl, and temperature for α-chymotrypsinogen A, Journal of Pharmaceutical Sciences 99 (2010) 645–662.
[23] A. Fernandez-Escamilla, F. Rousseau, J. Schymkowitz, L. Serrano, Prediction of sequence-dependent and mutational effects on the aggregation of peptides and proteins, Nature Biotechnology 22 (2004) 1302–1306.
[24] S.A. Tobler, B.W. Holmes, M.E.M. Cromwell, E.J. Fernandez, Benzyl alcohol-induced destabilization of interferon-γ: a study by hydrogen-deuterium isotope exchange, Journal of Pharmaceutical Sciences 93 (2004) 1605–1617.
[25] R. Hagen, R. Behrends, U. Kaatze, Acoustical properties of aqueous solutions of urea: reference data for the ultrasonic spectrometry of liquids, Journal of Chemical and Engineering Data 49 (2004) 988–991.
[26] P.L. Privalov, Stability of proteins, Advances in Protein Chemistry 33 (1979) 167–241.
[27] T.V. Chalikian, J. Volker, D. Anafi, K.J. Breslauer, The native and the heat-induced denatured states of alpha-chymotrypsinogen A: thermodynamic and spectroscopic studies, Journal of Molecular Biology 274 (1997) 237–252.
[28] J.M. Andrews, C.J. Roberts, A Lumry–Eyring nucleated polymerization model of protein aggregation kinetics: 1. Aggregation with pre-equilibrated unfolding, The Journal of Physical Chemistry. B 111 (2007) 7897–7913.
[29] Y. Li, C.J. Roberts, Lumry–Eyring nucleated-polymerization model of protein aggregation kinetics. 2. Competing growth via condensation and chain polymerization, The Journal of Physical Chemistry. B 113 (2009) 7020–7032.
[30] K.G. Denbigh, The Principles of Chemical Equilibrium: With Applications in Chemistry and Chemical Engineering, 4th ed. Cambridge University Press, 1981.
[31] M. Auton, D.W. Bolen, Predicting the energetics of osmolyte-induced protein folding/unfolding, Proceedings of the National Academy of Sciences of the United States of America 102 (2005) 15065–15068.
[32] J.K. Myers, C.N. Pace, J.M. Scholtz, Denaturant m values and heat capacity changes: relation to changes in accessible surface areas of protein unfolding, Protein Science 4 (1995) 2138–2148.
[33] C.J. Roberts, Non-native protein aggregation kinetics, Biotechnology and Bioengineering 98 (2007) 927–938.
[34] R. Rudolph, H. Lilie, In vitro folding of inclusion body proteins, The FASEB Journal 10 (1996) 49–56.